Earth-Science Reviews 220 (2021) 103723

Contents lists available at ScienceDirect

Earth-Science Reviews

journal homepage: www.elsevier.com/locate/earscirev

Rates of geological processes

Philip D. Gingerich *

Department of Earth and Environmental Sciences and Museum of Paleontology, University of Michigan, Ann Arbor, MI 48108-2228, USA

ARTICLE INFO

Keywords:
Temporal scaling
Log-difference-interval LDI plot
Log-rate-interval LRI plot
Fault creep
Carbon emissions
Glacial advance
Sediment accumulation
Tectonic uplift
River incision
Outcrop and basin erosion
Temperature change
Species extinction

ABSTRACT

Rates are widely used to characterize processes in the geological sciences, and the ratios that rates represent deserve more careful attention. The numerator is a measure of change or difference, and the denominator is generally a corresponding interval of time. Temporal scaling is the quantitative relationship of differences and rates to their associated time intervals. These relationships are proportional and appropriately studied on logarithmic axes. Here log-difference-interval (LDI) and log-rate-interval (LRI) graphs are analyzed for nine empirical case studies involving creep on the San Andreas Fault, anthropogenic carbon emissions, glacial advance and retreat, sediment accumulation, tectonic uplift and exhumation, river incision, beryllium-10 dating of outcrop and basin erosion, climate-related temperature change, and species-level extinction.

Two studies, fault creep and carbon emissions, are directional in the sense that each has observed differences changing in proportion to their associated time intervals; calculated rates are consequently independent of their denominators. The remaining studies are random or stationary in having differences that are independent to some degree from their associated intervals, and rates that are consequently dependent on their denominators. Rates dependent on denominators are common in geological studies because observed changes or differences are often constrained to a relatively narrow range compared to the much longer spans of time over which geological rates are calculated. When LDI or LRI temporal scaling shows change to fit a random or stationary model, meaning rates are dependent on their denominators, then any comparison of the rates involved must be restricted to, or projected to, some common denominator or common scale of time.

Radionuclide calibration of outcrop and basin erosion, and biological extinction are two stationary processes where rates are often compared, erroneously, on different scales of time.

1. Introduction

Zedeněk Kukal's 1990 book-length review titled *The Rate of Geological Processes* hinted that our understanding of geological rates changed in the 1980s. Kukal (1990, p. 122) first wrote of sedimentation: "The present is slightly anomalous because it is post-orogenic and post-glacial. Different conditions prevailed during most periods of geological history, and sedimentation was, on the average, slower." The idea that sedimentation, or any process, was slower in the past than today is the non-uniformitarian view of a rate literalist. But then Kukal pivoted: "The rate of sedimentation of ancient deposits has to be expressed over long periods of time, whereas recent sedimentation may be measured over shorter periods. As is now well known, the longer the period of observation, the more intervals of non-deposition it includes." Kukal cited Hans-Erich Reineck (1960) and Peter Sadler (1981) as evidence, transitioning to a more uniformitarian view that rates are influenced by the intervals of time they represent.

Rates are ratios, with a numerator and denominator. The numerator is a measure of change or difference, and the denominator is generally a corresponding interval of time. Rates are calculated to characterize processes and, in effect, standardize the numerator with respect to the denominator. Stand-alone rates are efficient and representative in some instances, but can be misleading in others. Rates are widely used to characterize processes in the geological sciences, and the ratios that rates represent deserve more attention.

Differences and rates both have a 'time scale,' which is the interval of time the observations of interest represent. If x_1 is an observation representing time t_1, and x_2 is an observation representing time t_2, then the change or difference in the observations is $D = x_2 - x_1$, which has an associated time scale or interval $I = t_2 - t_1$ (terms are summarized in Table 1). The rate of change is then $R = D / I = x_2 - x_1 / t_2 - t_1$, which has the same associated time interval or scale. The time scale is the denominator in a rate calculation. Here, when appropriate, the intervals associated with differences and rates are enclosed in chevrons or angled

* Corresponding author.
E-mail address: gingeric@umich.edu.

https://doi.org/10.1016/j.earscirev.2021.103723
Received 21 March 2021; Received in revised form 20 May 2021; Accepted 20 June 2021
Available online 24 June 2021

Table 1
Definition of terms.

Abbreviation	Definition
I	Interval of time or time scale, e.g., $t_2 - t_1$ ($I = D / R$)
D	Difference or amount of change, e.g., $x_2 - x_1$ ($D = I \cdot R$)
R	Rate of change, e.g., $x_2 - x_1 / t_2 - t_1$ ($R = D / I$)
$< I >$	Time scale associated with a calculated difference or rate
LI	Log_{10} value of an interval or time scale (LI = LD – LR)
LI span	Span of LI values (LImax – LImin)
LD	Log_{10} value of a difference (LD = LI + LR)
LD_0	LD intercept value when LI = 0
LD span	Span of LD values (LDmax – LDmin)
LR	Log_{10} value of a rate (LR = LD – LI)
LR_0	LR intercept value when LI = 0
LR span	Span of LR values (LRmax – LRmin)
LDI plot	Log-difference-interval graph (plotting log_{10} difference versus log_{10} interval)
LRI plot	Log-rate-interval graph (plotting log_{10} rate versus log_{10} interval)
n	Number of samples in a time series
N	Number of intervals, differences, and rates in a study
E	Number of species extinctions
E/MS	Number of species extinctions per million species
E/MSY	Number of species extinctions per million species years

brackets, as $< I >$, to set them off and emphasize their importance.

'Temporal scaling' as a noun is the quantitative relationship of differences to their associated intervals, or of rates to their associated intervals. This relationship is proportional and generally studied on logarithmic axes. Temporal scaling as a verb is an application of this relationship, through interpolation or extrapolation, to predict differences or rates for comparison on different scales of time. Evolutionary studies have shown that temporal scalings of differences and rates characterize patterns on a spectrum ranging from steady 'directional' change, where differences increase as the interval of time involved increases; to a steady or unsteady 'stationary' state of no net change with the passage of time (Gingerich, 1983, 1993, 2019b). Random change is an intermediate expectation, a cumulative time series summing successive $\pm \boldsymbol{n}(\mu, \sigma)$ drawn from a normal distribution with mean $\mu = 0$ and finite standard deviation σ. Random change can involve repeated reversals of directional change or some intermediate mixture of directional change and stasis as the associated time interval increases.

Temporal scaling can be studied on a log-difference-interval (LDI) graph, or on a log-rate-interval (LRI) graph. Logarithms are involved because the scaling of differences with intervals and the scaling of rates with intervals are relationships of proportion. Base-10 logarithms are convenient because they represent log interval (*LI*), log difference (*LD*), and log rate (*LR*) as orders of magnitude. Some differences and rates are calculated from longitudinal time series of observations where intervals may overlap. Other differences and rates are calculated from cross-sectional comparisons of paired observations, which are effectively one-step time series. Both provide comparable information on interval *I*, difference *D*, and rate *R*.

LDI and LRI graphs are different, but both tell us the same thing about rates and their temporal scaling in a study. LDI and LRI slopes are complementary in that the latter slope is always one unit more negative than the former. LDI and LRI intercepts are always the same. The advantage of an LRI graph is that it shows rates explicitly. Schlager et al. (1998) and Sheets and Mitchell (2001) argued that the inverse dependence of rate on interval is an artifact produced by spurious self-correlation. Anyone worried that plotting a rate against its denominator on an LRI plot is misleading can retrieve the scaling information from an LDI plot. Here LDI and LRI plots are shown side-by-side for each case study to make this point. Jerolmack and Sadler (2007), Gingerich (2009), Sadler and Jerolmack (2015), and Gingerich (2019a) made similar comparisons of LDI and LRI plots.

In the following case studies I calculate rates in nine geological settings, analyzing data compiled by others. The studies involve fault creep, carbon emissions, glacial advance and retreat, sediment accumulation, tectonic uplift and exhumation, river incision, outcrop and basin erosion, climate-related temperature change, and species-level extinction. The first two cases, fault creep and carbon emissions, are examples of stand-alone rates providing reliable general information, but the remaining seven studies involve rates that are misleading when separated from their denominators. The key question in any rate study is an empirical one: are the rates of interest independent of their time scale? When rates are independent they can be compared over a wide range of time scales. When rates remain dependent on their denominators the only reliable comparisons are those on the same scale of time, or those projected to the same scale of time.

2. Case studies

2.1. Fault Creep

Creep meters have been installed across active geological faults at many sites in California. One of these sites, Melendy Ranch, on the San Andreas Fault has measured creep since 1969 (Schulz, 1989). A sample of 191 creep measurements is analyzed here (Fig. 1A), spanning the 45-year interval from 1969 through 2014. During this time movement on the San Andreas fault totaled 772.81 mm, for an average rate of 17.27 mm per year calculated as a linear regression slope. This we can write as 17.27 mm / yr <45 yr>. The interval in chevrons is a reminder that the rate expressed per year was actually calculated over a 45-year interval.

It is also possible to calculate differences and rates on finer scales of time, as, for example, from sample 1 to sample 2, from 2 to 3, 3 to 4, etc., and then from sample 1 to sample 3, from 2 to 4, 3 to 5, etc. Exhaustive 'full-sample' calculation of differences and rates of change on all scales of time yields a total of $N = 0.5 \cdot n \cdot (n - 1)$ intervals, differences, and rates, where n is the number of successive samples in the time series. For the Melendy Ranch fault-creep series of $n = 191$ samples, we expect a total of $N = 18{,}145$ intervals, differences, and rates.

The full sample of Melendy Ranch intervals and corresponding differences is plotted on logarithmic axes in the LDI plot of Fig. 1B. There are 18,142 proportional differences plotted in Fig. 1B, not 18,145, because differences between three pairs of samples were zero on the scale of measurement, meaning their proportions were undefined. Absolute differences are plotted because signs of the differences do not affect their scaling.

Two features of the LDI plot in Fig. 1B are important. First, the median slope of a robust-linear-modeling line fit to the differences and intervals is 0.978, which is similar to the slope of 1.000 expected for a purely directional-process model and much different from the slope of 0.500 expected for a random model and from the slope of 0.000 expected for a purely stationary model. This makes sense because the plot of fault creep through time in Fig. 1A is clearly directional. A sample count of $N = 18{,}142$ is so large that bootstrapped confidence intervals (1000 replications) show 0.978 to be significantly different from 1.000 (single asterisk in Fig. 1B) and significantly different from both 0.500 and 0.000 (paired asterisks). Creep on the San Andreas Fault is not purely directional but is very close to this, with a very small random or stationary component. The second feature important in Fig. 1B is the median intercept of the robust-linear-modeling fit, 1.269, which, when exponentiated, corresponds to a difference of 18.57 mm on a time scale of 1 year.

The same information can be extracted from the LRI plot in Fig. 1C. First, the slope of a robust-linear-modeling line fit to the rates and intervals is −0.022, which is similar to the slope of 0.000 expected for a purely directional-process model and much different from the slope of −0.500 expected for a random model and from the slope of −1.000 expected for a purely stationary model. Here again, the sample count of $N = 18{,}142$ is so large that bootstrapped confidence intervals show −0.022 to be significantly different from 0.000 (single asterisk in Fig. 1C) and significantly different from both −0.500 and −1.000 (paired asterisks). The intercept in Fig. 1C is again 1.269, which, exponentiated,

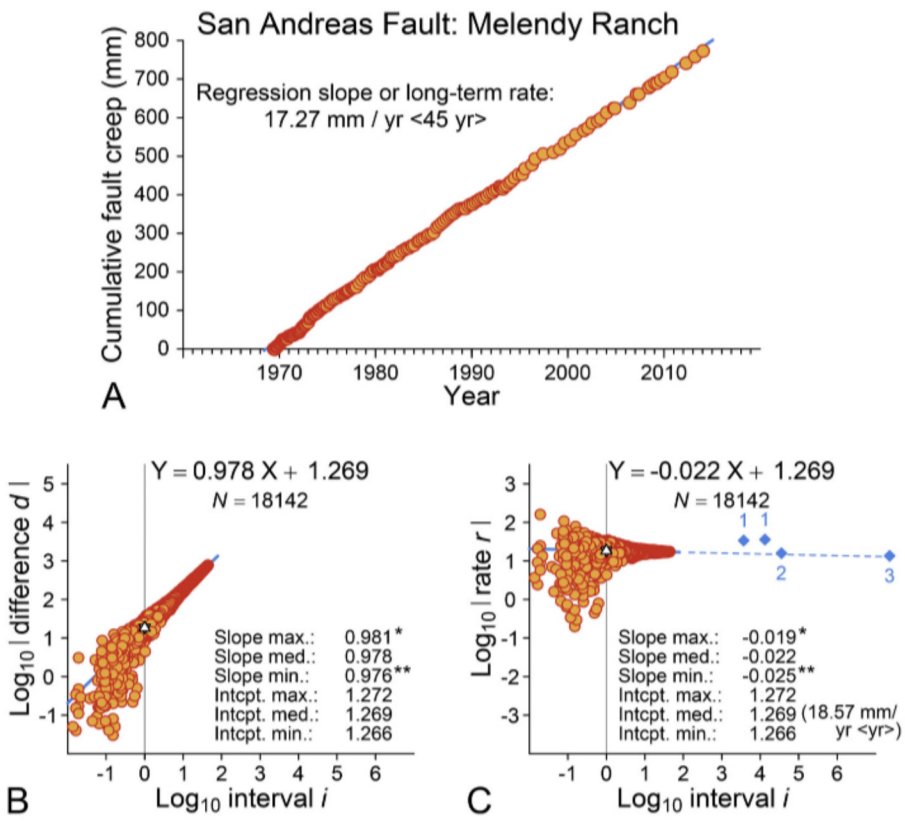

Fig. 1. Creep movement of the San Andreas Fault at Melendy Ranch in central California (Schulz, 1989). (A) Cumulative creep of the fault in historical times relative to its position in the year 1969 (https://earthquake.usgs.gov/monitoring/deformation/data/download.php). Blue line in the background is a linear regression fit to successive points. The slope is 17.27 mm / yr calculated over an interval of 45 years. (B) Log-difference-interval or LDI plot showing fault creep or difference (mm) on all time intervals of measurement (interval in years). (C) Log-rate-interval or LRI plot showing all rates of change (mm / yr) in relation to their corresponding intervals (interval in years). These are longitudinal differences and rates for a multistep time series. Blue lines in in the background in panels B and C are robust-linear-model fits, with intercepts calculated on a time scale of years. The slopes in each plot show that San Andreas Fault creep has been directional but significantly different from purely directional change (single asterisk). It is also significantly different from expectation for random change and for a purely stationary time series (paired asterisks). The stand-alone rates here are largely independent of their denominators. Rates for long-term movements on the fault (filled blue diamonds; see text) are consistent with the rates of shorter-term observations. (For interpretation of the references to colour in this figure legend, the reader is referred to the web version of this article.)

corresponds to a rate of 18.57 mm per year on a time scale of 1 year. Note that this is not very different from the Fig. 1A regression rate of 17.27 mm per year on a time scale of 45 years.

There are several long-term tests of fault creep on the San Andreas Fault as a purely directional model. Sieh and Jahns (1984) calculated average slip rates for the San Andreas Fault of 33.9 mm / yr on a time scale of 3900 years, and 35.8 mm / yr on a time scale of 13,250 years. The Sieh-Jahns rates and their corresponding time intervals are plotted as diamonds labeled '1' in Fig. 1C. Woerd et al. (2006) calculated an average slip rate for the San Andreas Fault of 15.9 mm / yr on a time scale of 35,500 years. The Woerd and others rate and its corresponding time interval are represented by the diamond labeled '2' in Fig. 1C. Finally, Revenaugh and Reasoner (1997) recorded 315 km of slip on the San Andreas fault during an interval of 23.1 million years, which correspond to an average slip rate of about 13.6 mm / yr on a time scale of 23.1 my. The Revenaugh-Reasoner rate and its corresponding time interval are plotted as the diamond labeled '3' in Fig. 1C.

Note that all four diamonds in Fig. 1C, representing long-term slip rates for the San Andreas Fault, lie on or near a projected extension of the line fitting the creep rates calculated from observations at Melendy Ranch. Short-term rates of creep and and long-term rates of slip on the San Andreas Fault are, to a close approximation, independent of their time scale, and they can be compared across a broad range of time scales. A rate of 18.57 mm / yr <yr> is little different from 17.27 mm / yr <45 yr>, or 35.8 mm / yr <13.25 kyr > or 13.6 mm / yr <23.1 my>. These San Andreas fault rates epitomize what we expect rates to be. This will become clearer as we calculate and compare rates for other geological processes.

2.2. Anthropogenic carbon emissions

The Paleocene-Eocene thermal maximum (PETM) is one of the rare, large, and rapid climate transients of the Cenozoic era, and it had a profound and lasting effect on the earth's marine and continental biota (Zachos et al., 2001). This global greenhouse warming event 56 million years ago was accompanied by, and seemingly caused by, substantial release of isotopically light carbon into the ocean and atmosphere (Dickens et al., 1995). The PETM is important environmentally as an example of global greenhouse warming deep in the geological past, and it is interesting to compare the anthropogenic release of carbon to the atmosphere today with estimates of carbon accumulation during onset of the PETM.

Modern carbon release rates are known for the years 1959 through 2018, a time series of 60 successive values spanning 59 years (Fig. 2A). Masses of carbon are measured in petagrams, where one petagram of carbon (PgC) is equivalent to 10^{15} g or 10^{12} kg or 10^{9} metric tons. Release rates have risen steadily, from 2.417 PgC per year in 1959, to 9.982 Pg C per year in 2018. This is an average increase of about 0.12 PgC / year and a fourfold increase in 59 years (Friedlingstein et al., 2019). Fig. 2A shows differences and rates for carbon release on a time scale of one year, and we can calculate additional differences and rates for intervals ranging from 2 to 3 … to 59 years (Fig. 2B, C). Here for $n = 60$ samples, we expect a total of $N = 0.5 \cdot n \cdot (n + 1) = 1830$ intervals, differences, and rates, and that is what we find.

The median slope of a weighted robust-linear-modeling fit to the differences and intervals in the LDI plot of Fig. 2B is 1.001, which is virtually identical to the slope of 1.000 expected for a directional-process model. Bootstrapping shows the observed slope to be significantly greater than a slope of 0.500 expected for a random model or the slope of 0.000 expected for a stationary model (paired asterisks). Similarly, the slope of a line fit to the rates and intervals in the LRI plot of Fig. 2C is 0.001, which is virtually identical to the slope of 0.000 expected for a directional-process model. Here again it is significantly greater than the slope of −0.500 expected for a random model or the slope of −1.000 expected for a stationary model (paired asterisks).

The median intercepts of the lines fit to the differences Fig. 2B and rates in Fig. 2C are 0.768, which, exponentiated, correspond to a difference of 5.86 PgC and a rate of 5.86 PgC / yr, both on a time scale of

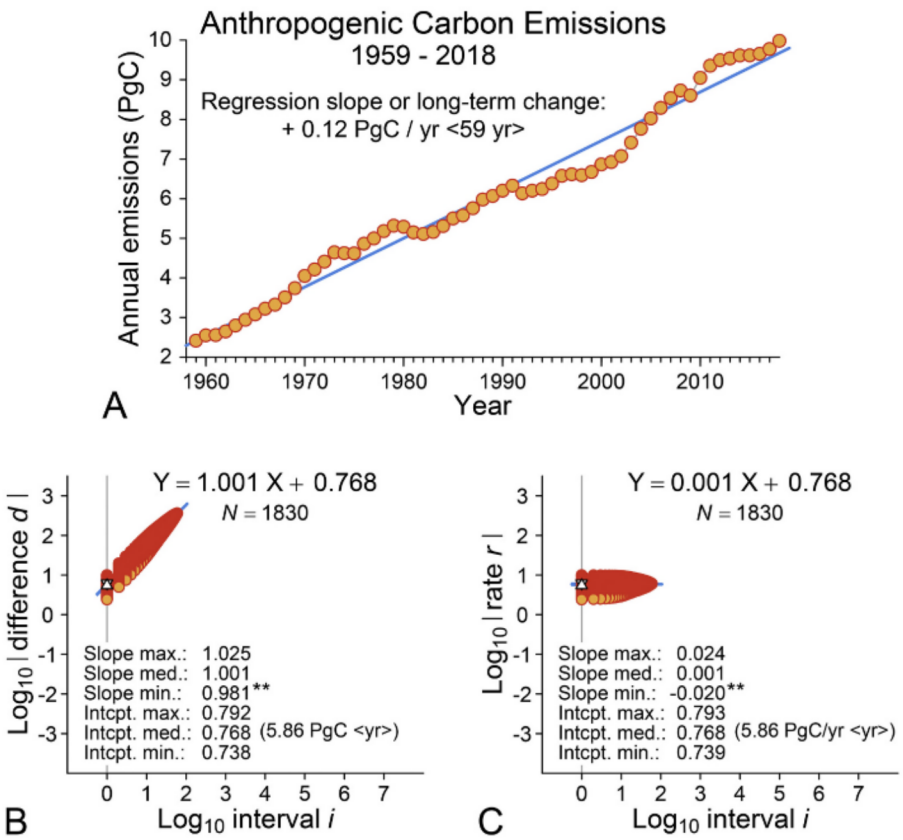

Fig. 2. Anthropogenic carbon emissions (Friedlingstein et al., 2019). (A) Emissions for individual years from 1959 through 2018. Blue line is a linear regression fit to emissions for successive years. The slope is 0.12 PgC / yr calculated over an interval of 59 years, showing that emissions increased through the interval studied. (B) Log-difference-interval or LDI plot showing emission rates (PgC) in relation to their corresponding intervals (intervals in years). (C) Log-rate-interval or LRI plot showing all rates of change (PgC / yr) in relation to their corresponding intervals (intervals in years). Blue lines in B and C are weighted robust-linear-model fits, with intercepts calculated on a time scale of years. The slopes in each plot show that carbon emissions are indistinguishable from expectation for a directional process, but significantly different from expectation for random change or a stationary time series (paired asterisks). The stand-alone rates here are largely independent of their denominators. If the present trend continues, carbon emissions are expected to reach a Paleocene-Eocene Thermal Maximum accumulation in 140 to 259 years or about 5 to 10 human generations (Gingerich, 2019a). (For interpretation of the references to colour in this figure legend, the reader is referred to the web version of this article.)

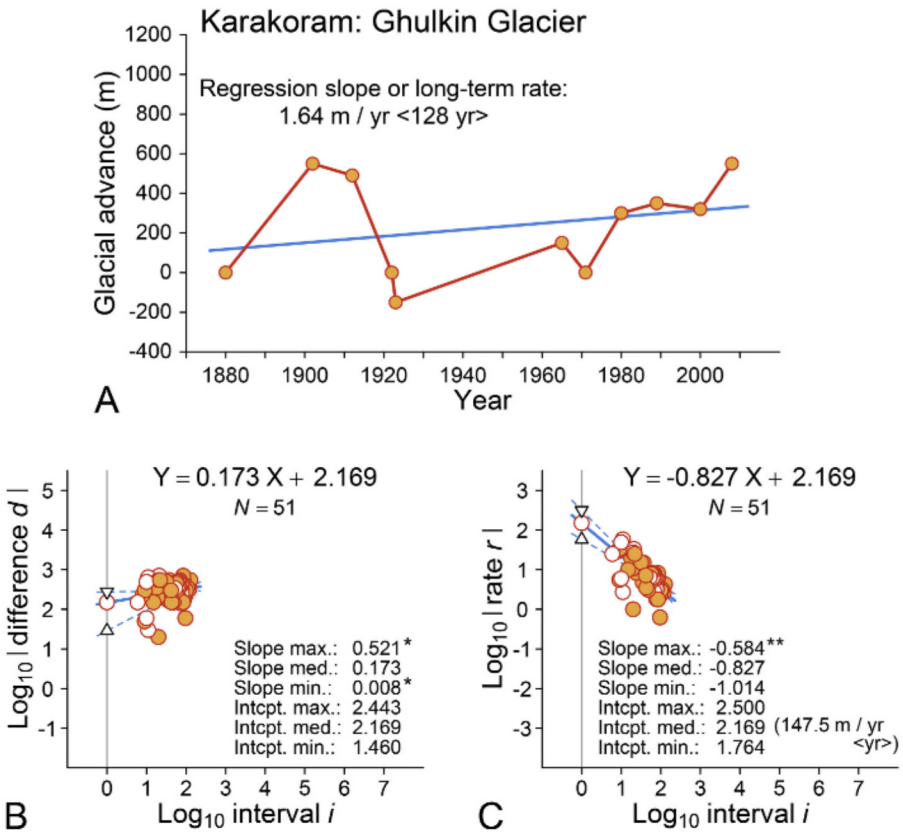

Fig. 3. Advances and retreats of the Ghulkin glacier in the Karakoram Range of northern Pakistan (Hewitt, 2011; Bolch et al., 2012). (A) Terminal positions of the glacier in historical times relative to its position in the year 1880. Blue line is a linear regression fit to the points. The slope is 1.64 m / yr calculated over an interval of 128 years. (B) Log-difference-interval plot showing glacial advances (m; filled circles) and retreats (open circles) in relation to the time interval (years) over which each is measured. (C) Log-rate-interval plot showing rates of change (m / yr) in relation to the corresponding interval (years). Blue lines are robust-linear-model fits, with intercepts calculated on a time scale of years. Maximum and minimum values are 95% confidence limits (dashed lines). These are longitudinal differences and rates for a multistep time series. The slopes in each plot show that Ghulkin glacial advance has been nearly stationary (not purely stationary) and significantly different from expectation for directional change (single asterisk in Fig. 3B) and from expectation for random and directional change (paired asterisks in Fig. 3C). Rates of change in glacial advance and retreat are dependent on their denominators, and when compared must be compared on the same scale of time. (For interpretation of the references to colour in this figure legend, the reader is referred to the web version of this article.)

one year. A rate of 5.86 PgC / yr <yr> is about average for all of the annual carbon emissions plotted in Fig. 2A. What is striking about this exercise is the directionality of the carbon emission process reflected in the LDI and LRI slopes (Fig. 2B, C). Anthropogenic emissions are rising at about 0.12 PgC each year. If this trend continues, we can expect to reach a PETM-scale accumulation of atmospheric carbon in as few as 140 to 259 years, which is about 5 to 10 human generations (Gingerich, 2019a).

2.3. Glacial advance and retreat

Tobias Bolch and others published a review of Himalayan and Karakoram glaciers in 2012. Most have retreated and lost mass since the mid-19th century, but movement of the Ghulkin glacier in the Karakoram Range of northern Pakistan is more complicated (Fig. 3A) and it has advanced during this time (Hewitt, 2011). Bolch et al. (2012) compared terminal positions of Ghulkin in 1880 and 2008, and listed the rate of a 550 m advance as 4.3 m per annum. A similar calculation based on regression of successive terminal positions on time (Fig. 3A) yields a slightly more modest average rate of 1.64 m per annum. In the terminology adopted here this is 1.64 m / yr <128 yr > to indicate that it is a rate calculated over an interval of 128 years.

Here again we can calculate differences and rates on finer time scales. For the Ghulkin glacier series of $n = 11$ records, we expect a total of $N = 0.5 \cdot n \cdot (n - 1) = 55$ intervals, differences, and rates. Differences between four pairs of samples were zero on the scale of measurement, and the number of intervals, differences, and rates available for analysis was thus 51.

The median slope of a robust-linear-modeling fit to the differences and intervals in the LDI plot of Fig. 3B is 0.173, which is more similar to the slope of 0.000 expected for a stationary-process model than it is to the slope of 0.500 expected for a random model or the slope of 1.000 expected for a purely directional model. Similarly, the slope of a line fit to the rates and intervals in the LRI plot of Fig. 3C is −0.827, which is more similar to the slope of −1.000 expected for a stationary-process model than it is to the slope of −0.500 expected for a random model or the slope of 0.000 expected for a purely directional model. A sample count of $N = 51$ is small enough that bootstrapped confidence intervals (1000 replications) show 0.173 to be significantly different from 0.0500 and 1.000 (paired asterisks in Fig. 3B), but not from 0.000. Bootstrapped confidence intervals show −0.827 to be significantly different from 0.000 (asterisk in Fig. 3C) but not from −0.500 or − 1.000. Temporal scaling of differences and rates in Fig. 3B and C indicate that Ghulkin glacial advance through time is stationary with a random component.

The median intercepts of the robust-linear-modeling fits in Fig. 3B and C are 2.169, which, when exponentiated, correspond to a difference of 147.5 m on a time scale of one year and to a rate of 147.5 m / yr on a time scale of one year. This rate of 147 m / yr <yr> is much higher than the rate of 1.64 m / yr <128 yr > calculated by regression over the whole time interval. Rates of Ghulkin glacial advance and retreat differ from creep observed on the San Andreas fault and from anthropogenic carbon emissions in being more sensitive to interval length. Ghulkin glacial movement is much more rapid on shorter scales of time than it is on longer scales of time. The denominator is an auxiliary but integral component of the rate, and the rate must be interpreted in the context of its time scale.

2.4. Sediment accumulation

Peter Sadler was the first to show, clearly and convincingly, that rates of sediment accumulation are inversely proportional to the intervals of time they represent. Sadler (1981) compiled nearly 25,000 rates and graphed these in bins relative to their denominators. The binned rates are shown on a log-rate-interval plot in Fig. 4B. From Sadler's key and the total number of rates we can infer that his bin colors represent about 5, 10, 20, 40, and 110 rates, respectively (the actual numbers of rates in each bin were not archived). Some of Sadler's rates are not longitudinal like those from multi-step time series analyzed above, but rather are cross-sectional rates calculated from differences in thickness in what are effectively one-step time series. Given Sadler's LRI graph we can back-calculate the corresponding log-difference-interval or LDI plot, which is shown in Fig. 4A.

The median slope of a frequency-weighted robust-linear-modeling fit to the differences and intervals in the LDI plot of Fig. 4A is 0.392. This is more similar to the slope of 0.500 expected for a random-process model than it is to the slope of 0.000 expected for a purely stationary model or to the slope of 1.000 expected for a purely directional model. The slope of a line fit to the rates and intervals in the LRI plot of Fig. 4B is −0.608, which is more similar to the slope of −0.500 expected for a random-process model than it is to the slope of −1.000 expected for a purely stationary model or to the slope of 0.000 expected for a purely directional model. A sample count N approaching 25,000 is large enough that bootstrapped confidence intervals (1000 replications) show the LDI and LRI slopes to be significantly different from expectation for purely stationary, random, or directional change (asterisks in Fig. 4A and b). The slopes themselves indicate that sediment accumulation through time is a

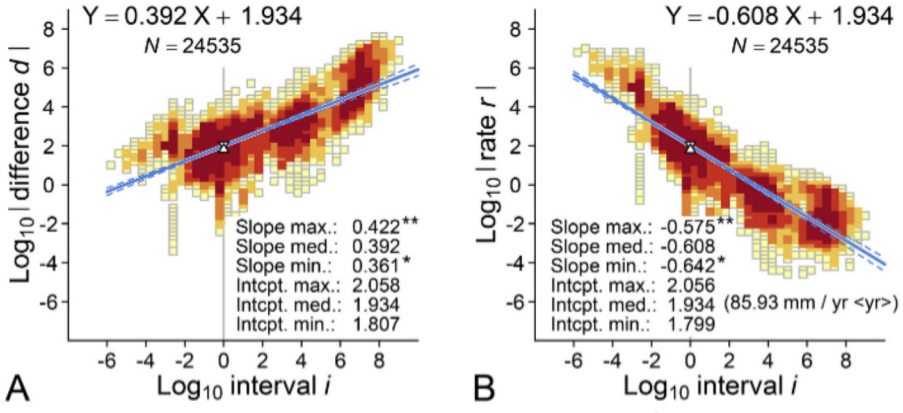

Fig. 4. Sediment accumulation on time scales ranging from minutes to millions of years (Sadler, 1981). Nearly 25,000 observations shown here are cross-sectional differences and rates for one-step time series. Lighter squares have fewer and darker squares have more differences and rates. (A) Log-difference-interval plot showing sediment accumulation (mm) in relation to the time over which each difference was calculated (years). (B) Log-rate-interval plot showing rates of sediment accumulation (mm / yr) in relation to the corresponding interval. Blue lines are robust-linear-model fits weighted by colour (5, 10, 20, 40, and 110), with intercepts calculated on a time scale of years. Maximum and minimum values are 95% confidence limits (dashed lines). The slopes in each plot show that sediment accumulation as a process scales on the stationary side of random and differs significantly from a purely stationary model (single asterisk) and from random and purely directional models (paired asterisks). A stationary model may be a better fit for short-term sediment accumulation and a random model a better fit for long-term sediment accumulation. Either way, rates of sediment accumulation are dependent on their denominators, and when compared must be compared on the same time scale. (For interpretation of the references to colour in this figure legend, the reader is referred to the web version of this article.)

more-or-less random process with a stationary component. The stationary component results from the narrower range of measurable differences relative to the range of associated time intervals (see Discussion). Residual differences in Fig. 4A and B span about eight orders of magnitude, while associated time intervals span some 15 orders of magnitude.

The median intercepts for the robust-linear-modeling fits in Fig. 4A and B are 1.934, which, when exponentiated, correspond to a difference of 85.93 mm on a time scale of one year and a rate of 85.93 mm / yr on a time scale of one year. Sadler (1981) reported sediment accumulation rates in units of m / 1000 yr, which has an equivalent rate intercept of 85.93 m / 1000 yr < yr>. The intercept on a time scale of a million years would be much different at 0.019 mm / yr <10^6 yr>, or 0.019 m / 1000 yr <10^6 yr>. Sediment accumulation is much more rapid on shorter scales of time than it is on longer scales of time. Taken to the limit, single-grain arrivals add one grain of sediment in an instant, and the rate of accumulation is effectively infinite. Rates of sediment accumulation separated from their denominators or underlying time scale are likely to be misleading, which is the reason for careful matching of time scales in the sediment-accumulation-rate comparisons of Partin and Sadler (2016). Other follow-up studies include Jerolmack and Sadler (2007), Sadler and Jerolmack (2015), and Aadland et al. (2018).

2.5. Tectonic uplift and exhumation

Thomas Gardner et al., (1987) published a study of geomorphic and tectonic process rates, following the rate studies of Sadler (1981) and Gingerich (1983). Gardner and colleagues employed LDI plots but avoided LRI plots, writing that spurious correlation might compromise direct comparison of rates with corresponding intervals. LDI and LRI plots are shown side by side in Fig. 5 to emphasize that they are consistent in providing the same information. Gardner et al. (1987) found that geomorphic and tectonic differences and rates, like sediment accumulation rates, are dependent on their associated time intervals. The original data of Gardner et al., have been lost (Gardner, personal communication), but Wilkinson et al. (2009) digitized the published Gardner graphs and added more observations from the literature. Analysis here is based on the sample of 754 tectonic uplift and exhumation rates and intervals of Wilkinson et al.

The Gardner et al. (1987) LDI plot and the Wilkinson et al. (2009) LRI plot are noisy in the sense that they have relatively great residual variation. The uplift and exhumation differences and rates were calculated on time scales ranging from less than a year to more than 10^8 years, a span of nearly nine orders of magnitude. Gardner et al., and Wilkinson et al., found clear dependence of differences and rates on their associated time intervals (Fig. 5A and B). Here, as in the Sadler study, the differences and rates are cross-sectional, calculated from measurements that are effectively one-step time series.

The median slope of a robust-linear-modeling fit to the differences and intervals in the LDI plot of Fig. 5A is 0.722. The corresponding slope in the LRI plot of Fig. 5B is −0.278. Each is intermediate between the slope expected for a purely directional-process model, and the slope expected for a random model. The sample count $N = 754$ is large enough that bootstrapped confidence intervals (1000 replications) show both slopes to be significantly different from expectation for purely stationary, random, or purely directional change (asterisks).

The median intercepts of the robust-linear-modeling fits in Fig. 5A and B are 1.031, which, when exponentiated, correspond to a difference of 10.7 mm / yr on a time scale of one year and a rate of 10.7 mm / yr on a time scale of one year. Rates of tectonic uplift and erosional exhumation are more rapid on shorter historical scales of time than they are on longer geological scales of time. Stand-alone rates of uplift and exhumation, separated from their denominators, are likely to be misleading.

2.6. River incision

Finnegan et al. (2014) reviewed rates of river incision and showed that most incision rates are dependent on their associated time intervals (denominators). One of their examples, incision of the Blue Nile in Ethiopia, was published by Gani et al. (2007), table DR1). The Blue Nile incision differences and rates recalculated here have time scales ranging from about 10^6 to $10^{7.5}$ years, a span of 1.5 orders of magnitude. Analyses on the LDI and LRI graphs of Fig. 6 confirm a clear dependence of incision differences and rates on their associated time intervals. Here, as in the Sadler (1981) and Gardner et al. (1987) studies, the differences and rates are cross-sectional, calculated from incisions that are effectively one-step time series.

The median slope of a robust-linear-modeling fit to the incision differences and intervals in Fig. 6A is 0.449. This is more similar to the slope of 0.500 expected for a random-process model than it is to the slope of 0.000 expected for a purely stationary model or the slope of 1.000 expected for a purely directional model. Similarly, the slope of a line fit to the rates and intervals in the LRI plot of Fig. 6B is −0.551, which is again similar to the slope of −0.500 expected for a random model. The observation count $N = 23$ is small, but bootstrapped confidence intervals (1000 replications) show both slopes to be significantly different from expectation for purely stationary, random, or purely

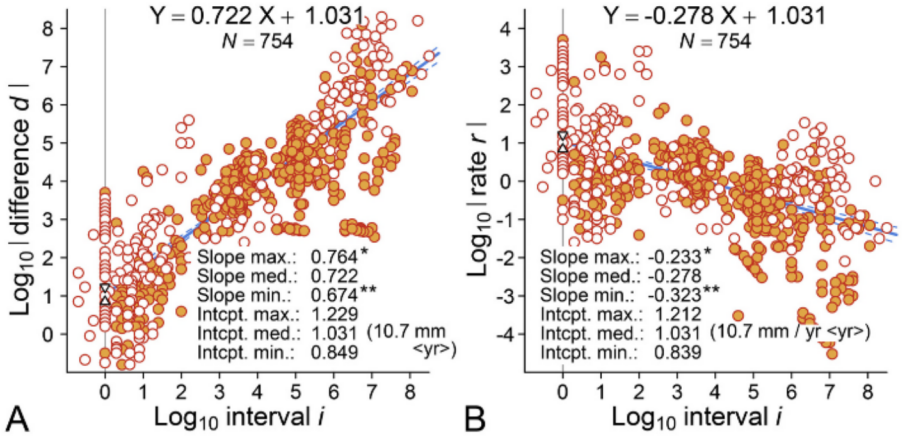

Fig. 5. Tectonic uplift and exhumation on time scales ranging from years to many millions of years (Wilkinson et al. (2009). These are cross-sectional differences and rates for one-step time series. Filled circles represent uplift; open circles exhumation. (A) Log-difference-interval plot showing change in uplift and exhumation (mm) in relation to the time over which each difference is calculated (years). (B) Log-rate-interval plot showing rates of uplift and exhumation (mm / yr) in relation to the corresponding interval. Blue lines are robust-linear-model fits, with intercepts calculated on a time scale of years. Maximum and minimum values are 95% confidence limits (dashed lines). The slopes in each plot show that tectonic change has been more directional than random or stationary, and significantly different from each model (asterisks). Rates of tectonic uplift and exhumation here are dependent on their denominators, and when compared must be compared on the same time scale. (For interpretation of the references to colour in this figure legend, the reader is referred to the web version of this article.)

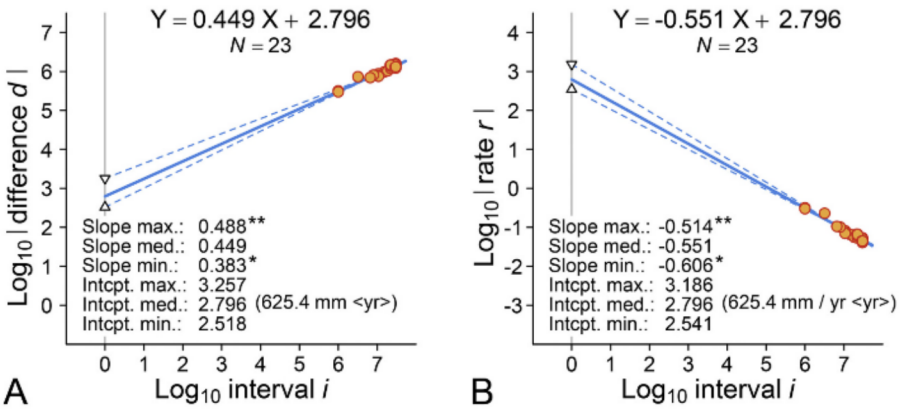

Fig. 6. River incision of the Blue Nile in Ethiopia on time scales ranging from a million to tens of millions of years (Gani et al., (2007). These are cross-sectional differences and rates for one-step time series. (A) Log-difference-interval plot showing river incision (mm) in relation to the time over which each difference is calculated (years). (B) Log-rate-interval plot showing rates of incision (mm / yr) in relation to the corresponding interval. Blue lines are robust-linear-model fits, with intercepts calculated on a time scale of years. Maximum and minimum values are 95% confidence limits (dashed lines). The slopes in each plot show that incision has been nearly random, but not purely random or directional (paired asterisks) and not stationary (asterisk). Rates of Blue Nile river incision are dependent on their denominators, and when compared must be compared on the same time scale. (For interpretation of the references to colour in this figure legend, the reader is referred to the web version of this article.)

directional change (asterisks in Fig. 6A and B). River incision through geological time is effectively random or a random combination of directional and stationary components. The range or span of LI time intervals is twice the span of Blue Nile LD incision differences, and the span of LI time intervals is about six times the range of LD and LR residuals.

The median intercepts of the robust-linear-modeling fits in Fig. 6A and B are 2.796, which, exponentiated, correspond to a difference of 625.4 mm on a time scale of one year and a rate of 625.4 mm / yr on a time scale of one year. The rate of Blue Nile incision is more rapid on shorter scales of time than it is on longer scales of time. Rates of river incision separated from their denominators are likely to be misleading.

2.7. Radionuclide calibration of outcrop and basin erosion

Devendra Lal was a pioneer in using the cosmogenic radionuclide beryllium-10 to estimate rates of erosion (Lal, 1991; Dunai, 2010). Portenga and Bierman (2011), in a global review, compared ^{10}Be erosion rates for rock outcrops to those for drainage basins. They found considerable overlap but concluded that drainage basins erode more rapidly on average than outcrops, and attributed the difference to more rapid rock weathering rates under soils. This idea can be tested by comparing erosion differences and rates for outcrops and basins in relation to their associated time scales.

^{10}Be decays with a half-life, $t_{½}$, variously estimated at about 1.36 to 1.50 million years, and a corresponding decay constant $\lambda = \ln(2) / t_{½}$. The steady-state erosion rate ε is a function of the density (ρ) of the target material, the absorption mean free path (Λ), the production rate of the radionuclide at sea level at high latitudes (P), the nuclide concentration (Nc), and the decay constant λ. Density and mean free path can be combined as an absorption coefficient $\mu = \rho / \Lambda$. The exposure interval or irradiation time for the rock or sediment surface is $T_{\text{eff}} = Nc / P$. Following Lal (1991) and Portenga and Bierman (2011), exposure rate ε can be calculated as:

$$\varepsilon = \frac{1}{\mu}\cdot\left[\frac{1}{T_{\text{eff}}} - \lambda\right] \text{ or } \varepsilon = \frac{\Lambda}{\rho}\cdot\left[\frac{P}{Nc} - \lambda\right] \quad (1)$$

Portenga and Bierman (2011) provided sources and the information required to recalculate erosion rates for studies and sites around the world. Their table DR1 includes summary values for ε, Λ, ρ, P, and $t_{½}$. The latter, $t_{½}$, can be used to calculate λ. Substitution in eq. 1 enables calculation of a summary value for Nc for many of the sites. Combination of Nc with P provides the interval $T_{\text{eff}} = Nc / P$ associated with each erosion rate ε. Data in table DR1 enable calculation of T_{eff} for 18 outcrop studies and 21 basin studies. These are analyzed in the LDI and LRI plots shown in Fig. 7.

The median slope of a robust-linear-modeling fit to the differences and intervals in the LDI plot of Fig. 7A is 0.020. This is more similar to the slope of 0.000 expected for a stationary-process model than it is to the slope of 0.500 expected for a random model or the slope of 1.000

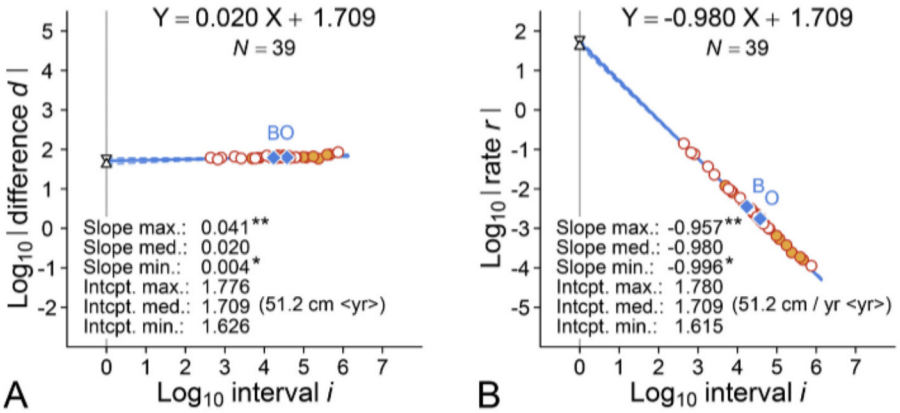

Fig. 7. Radionuclide-calibrated outcrop erosion (filled circles) and basin erosion (open circles) on time scales ranging from about one thousand to a million years (Portenga and Bierman, 2011). Each point is an average calculated from rock properties, cosmogenic production, and decay of the radionuclide ^{10}Be in one of 39 empirical studies. (A) Log-difference-interval plot of erosion amounts (cm) in relation to the time interval over which each is estimated (years). (B) Log-rate-interval plot of erosion rates (cm / yr) in relation to the corresponding interval. Blue lines are robust-linear-model fits, with intercepts calculated on a time scale of years. Maximum and minimum values are 95% confidence limits (dashed lines). The slopes in each plot show that erosion amounts have been nearly stationary, but not purely stationary (single asterisk), and not random or directional (paired asterisks). Blue diamonds show median basin (B) and outcrop (O) values for log interval length, log erosion amount, and log erosion rate. Basin and outcrop rates appear to be different, but the difference reflects their calculation and comparison on different scales of time. (For interpretation of the references to colour in this figure legend, the reader is referred to the web version of this article.)

expected for a purely directional model. Similarly, the slope of a line fit to the rates and intervals in the LRI plot of Fig. 7B is −0.980, which is more similar to the slope of −1.000 expected for a stationary-process model than it is to the slope of −0.500 expected for a random model or the slope of 0.000 expected for a purely directional model. The sample count $N = 39$ is large enough that bootstrapped confidence intervals (1000 replications) show both slopes to be significantly different from expectation for purely stationary, random, or purely directional change (asterisks in Fig. 7A and B). Slopes of the LDI and LRI plots indicate that erosion estimated from ^{10}Be is a nearly stationary process, with a very small random or directional component. The range of estimated erosion differences is negligible relative to the range of associated time intervals.

The median intercepts of the robust-linear-modeling fits in Fig. 7A and B are 1.709, which, when exponentiated, correspond to an erosion difference of 51.2 cm on a time scale of one year and an erosion rate of 51.2 cm / yr on a time scale of one year. More or less constant erosion differences across the investigated range of time scales (Fig. 7A) mean that associated erosion rates are inversely proportional to their denominators (Fig. 7B), representing different scales of time. Consequently very few of the rates can be compared on the same time scale. Portenga and Bierman (2011) attributed the relatively rapid erosion of drainage basins to more rapid weathering rates under soils. However, the difference between median basin rates and median outcrop rates (diamonds labeled 'B' and 'O' in Fig. 7B) is more easily explained as a result of comparison on different scales of time.

Finally, if erosion rates calculated from cosmogenic radionuclide ages cannot be compared to each other — because each is calculated on a different scale of time — then it makes little sense to compare one or more average cosmogenic erosion rates to one or more average thermochronometric erosion rates, as attempted by Ganti et al., (2016). Thermochronometric rates, like cosmogenic rates, are inversely proportional to their denominators, representing different scales of time, and any average thermochronometric rate again depends on its associated time scale. Thermochronometric rates with the same values as cosmogenic rates are calculated on time scales some four orders of magnitude greater than time scales of the cosmogenic rates, which, with scaling slopes of −1, means that the thermochronometric rates will be some four orders of magnitude greater than the cosmogenic rates when extrapolated to the same time scale. This is easily seen by plotting log erosion rate (mm / yr) against log age (yr) for all rates and sites in table S2 of Ganti et al., 2016.

2.8. Climate-related temperature change

David Kemp and co-authors compiled 194 examples of substantial temperature changes or differences and their associated rates in the geological record of climate and climate change. The temperature differences and rates were calculated on time scales ranging from about 10 to 10^8 years. Analysis on log-difference-interval and log-rate-interval graphs showed clear dependence of temperature differences and rates on their associated time intervals (Kemp et al., 2015; replotted here on the LDI graph of Fig. 8A and LRI graph of Fig. 8B). The differences and rates are cross-sectional, calculated from temperature changes that are effectively one-step time series.

The median slope of a robust-linear-modeling fit to the differences and intervals in the LDI plot of Fig. 8A is 0.120. This is more similar to the slope of 0.000 expected for a stationary-process model than it is to the slope of 0.500 expected for a random model or the slope of 1.000 expected for a purely directional model. Similarly, the slope of a line fit to the rates and intervals in the LRI plot of Fig. 8B is −0.880, which is more similar to the slope of −1.000 expected for a stationary-process model than it is to the slope of −0.500 expected for a random model or the slope of 0.000 expected for a purely directional model. The temperature-change count $N = 194$ is large enough that bootstrapped confidence intervals (1000 replications) show both slopes to be significantly different from expectation for purely stationary, random, or purely directional change (asterisks in Fig. 8A and B). Slopes of the LDI and LRI plots indicate that the process of temperature change through geological time is largely stationary, with a relatively small random or directional component. This is again attributable to the narrower range of observable temperature differences relative to the range of associated time intervals. Measured differences in Fig. 8A span just two orders of magnitude, while associated time intervals span some eight orders of magnitude.

The median intercepts of the robust-linear-modeling fits in Fig. 8A and B are −0.058, which, exponentiated, correspond to a difference of 0.9 °C on a time scale of one year and a rate of 0.9 °C / yr on a time scale of one year. Rates of temperature change are much more rapid on the shorter scales of time accessible historically today than they are on longer scales of time typically recorded in the geological past. Rates of temperature change separated from their denominators are likely to be misleading.

2.9. Species extinction

Rates of extinction of species in modern times are often compared to 'background' rates in the geological past. Pimm et al. (2006) introduced

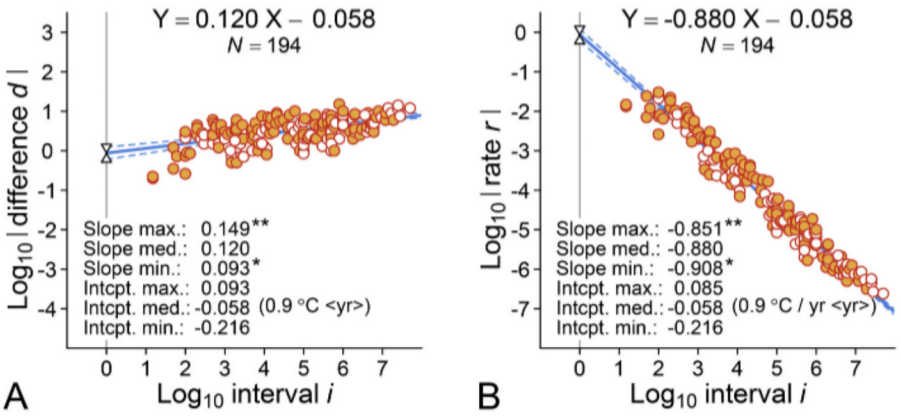

Fig. 8. Climate-related temperature change on time scales ranging from tens to many millions of years (Kemp et al., 2015). These are cross-sectional differences and rates for one-step time series. Filled circles represent positive change; open circles negative change. (A) Log-difference-interval plot showing temperature changes (°C) in relation to the time over which each is calculated (years). (B) Log-rate-interval plot showing rates of change in temperature (°C / yr) in relation to the corresponding interval. Blue lines are robust-linear-model fits, with intercepts calculated on a time scale of years. Maximum and minimum values are 95% confidence limits (dashed lines). The slopes in each plot show that temperature has been nearly stationary, but not purely stationary (single asterisk), and not random or directional (paired asterisks). Rates of change in temperature are dependent on their denominators, and when compared must be compared on the same time scale. (For interpretation of the references to colour in this figure legend, the reader is referred to the web version of this article.)

a metric involving the number of extinctions, E, in an interval, normalized by the million-species-years (MSY) involved, for an extinction rate E/MSY. Species that last 10^6 and 10^7 years before extinction were reported as having rates of 1 and 0.1 E/MSY, respectively, quantified on a time scale of years.

The online Paleobiology Database (PBDB; https://paleobiodb.org) includes stratigraphic ranges for many species that are now extinct. Here PBDB ranges for 9561 extinct Cenozoic mammal species are analyzed to quantify extinction rates in E/MSY. The species durations or ranges vary from a minimum of 114.3 thousand years to a maximum of 60.7 million years, with a median range or interval of 5.3 million years. Perceived minimum and median durations of species are sensitive to the temporal duration of sampling intervals and the calibration precision of geological time, but increased sampling and precision are unlikely to change the temporal scaling of extinction rates shown here.

The first interval of the PBDB with Cenozoic mammals is an early Paleocene interval ranging from 66.0 to 63.3 million years before present. This interval has 230 total species and spans 2.7 my, with 123 species confined to the interval and 107 surviving to a subsequent interval. The rate numerator or extinction difference is the proportion extinct in the interval, expressed as a proportion of a million species, here $123/230 \cdot 10^6 = 534{,}782$ extinctions per million species or E/MS. The rate denominator is the focal interval, here $2.7 \cdot 10^6$ years. The extinction rate is then the quotient of the numerator and denominator, as expressed in eq. 2. This is a rate on a time scale of $2.7 \cdot 10^6$ years:

$$\frac{123\ extinctions}{230\ total\ species} \cdot 10^6\ species \Big/ 2.7{\cdot}10^6\ years = 0.198\ E \Big/ MSY \qquad (2)$$

The second PBDB interval analyzed, ranging from 66.0 to 61.7 Ma, has 107 total species and spans 4.3 my, with 39 species confined to the interval and 68 surviving to a subsequent interval. The associated extinction rate is 0.085 E/MSY. This is a rate on a time scale of $4.3 \cdot 10^6$ years. Similar calculations, repeated for each individual interval and each combination of intervals, yield a total of 429 non-zero extinction differences and extinction rates on a broad range of time scales.

The 429 extinction differences for Cenozoic mammals are plotted on the log-difference-interval (LDI) plot in Fig. 9A, and the corresponding extinction rates are plotted on the log-rate-interval (LRI) plot in Fig. 9B. The proportion of species extinct has an upper limit of 1 because extinctions in an interval cannot exceed the number of species in the interval (this equivalence, when observed, is limited to intervals with very few species). The corresponding upper limit on the LDI plot is the log difference $LD_0 = \log_{10}(10^6\ \text{species}) = 6$. The median proportion of extinctions to total species in the PBDB sample of Cenozoic mammals is 0.417, and the corresponding median log difference, shown by the solid blue line in Fig. 9A, is $\log_{10}(416{,}869) = 5.62$. Lighter dashed lines show distribution quartiles for background extinction differences based on the Cenozoic species.

The extinction rates on the LRI plot in Fig. 9B have an upper limit $LR_0 = LD_0 - LI$, where LI is the $\log_{10}$ value of the corresponding interval in years. Here again the median proportion of extinctions to total species for Cenozoic mammals is 0.417 and the corresponding median extinction difference is $416{,}869 = 10^{5.62}$. The median log extinction rate LR = LD – LI is shown by the solid blue line in Fig. 9B. Lighter dashed lines show the corresponding distribution quartiles for background extinction rates.

Foote and Raup (1996) analyzed a compilation of 2941 Cenozoic mammal species in intervals of $0.7 \cdot 10^6$ years and calculated an extinction rate of 0.28 for the interval. The extinction difference as a proportion of a million species is $0.28 \cdot 10^6 = 280{,}000$ E/MS. Substituting in eq. 3, the background extinction rate is 0.40 E/MSY on a time scale of $0.7 \cdot 10^6$ years:

$$0.28{\cdot}10^6\ species / 0.7{\cdot}10^6\ years = 0.40\ E/MSY \qquad (3)$$

The extinction difference of Foote and Raup is plotted as the diamond labeled '1' on the LDI plot of Fig. 9A, and the background extinction rate of Foote and Raup is plotted as the diamond labeled '1'on the LRI plot of Fig. 9B. Both are close to the median background difference and rate calculated here from analysis of the PBDB data (solid blue lines).

The Cenozoic mammal extinction differences and rates in Fig. 9A and B provide background for interpretation of more modern extinction differences and rates representing shorter scales of time. Regan et al., (2001) calculated the rate of mammalian species extinctions over the past 400 years for comparison with the geological background rate of Foote and Raup. Regan and others considered the number of mammalian extinctions in the interval to be 60 out of a total of 4327 extant mammal species. This is a rate on a time scale of 400 years:

$$\frac{60\ extinctions}{4{,}327\ total\ species} \cdot 10^6\ species \Big/ 400\ years = 34.7\ E \Big/ MSY \qquad (4)$$

The extinction difference of Regan and others, 13,866 E/MS, is plotted versus the corresponding interval of 400 years on the LDI plot of Fig. 9A. Their extinction rate, 34.7 E/MSY calculated in eq. 4, is plotted versus the interval of 400 years on the LRI plot of Fig. 9B (each is a diamond labeled '2').

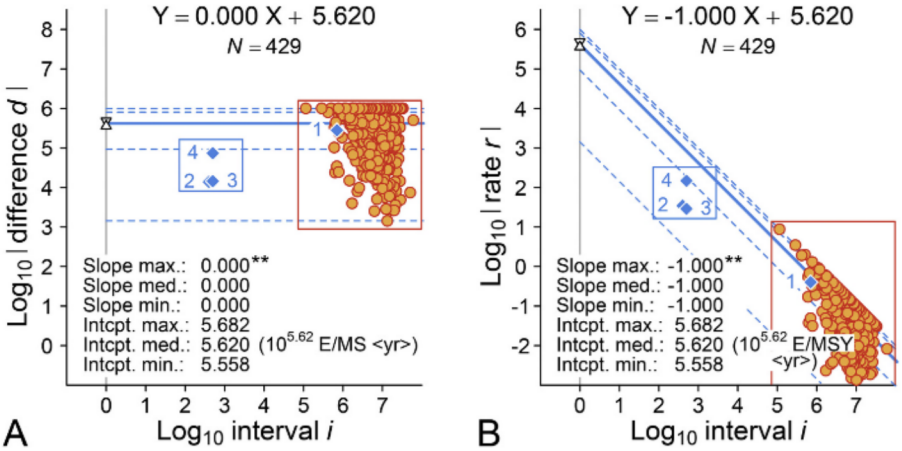

Fig. 9. Species extinctions of Cenozoic mammals on time scales ranging from 10^5 to 10^8 years. (A) LDI plot of species extinctions (extinctions per million species or E/MS) in relation to the associated time interval (years). (B) Log-rate-interval plot of extinction rates (extinctions per million species years or E/MSY) in relation to the corresponding time interval (years). Solid blue line in each plot is fit to median values with a slope of 0 or − 1 derived from the limiting cases. Dashed lines are quartiles. Maximum and minimum values for the intercepts are 95% confidence limits based on linear-model standard errors. The slopes in each plot show that extinction as a process is stationary and not random or directional (paired asterisks). Blue diamonds labeled '1' are from Foote and Raup (1996), and blue diamonds labeled '2' through '4' are extinction rates for mammals in modern times (see text). Rates of extinction are dependent on their denominators, and when compared must be compared on the same time scale. The rates for mammals in modern times are lower, not higher, than expected from the temporal scaling of background extinction differences and rates in the fossil record. (For interpretation of the references to colour in this figure legend, the reader is referred to the web version of this article.)

Regan and others considered 34.7 *E*/MSY to be about 87 times the background extinction rate of 0.4 *E*/MSY calculated from Foote and Raup (1996). However, this is a comparison based on different scales of time. The blue diamonds labeled '2' in Fig. 9A and B show the difference and rate of Regan and others to fall in the lower quartile of background differences and rates based on Cenozoic mammals, well below the median expectation for the time interval involved.

Barnosky et al., (2011) calculated a rate of modern mammal species extinctions in *E*/MSY with slightly different numbers from those of Regan and others:

$$\frac{80\ extinctions}{5570\ total\ species}\cdot 10^6\ species \Big/ 500\ years = 28.7\ E \Big/ MSY \quad (5)$$

The blue diamond labeled '3' in Fig. 9A shows the extinction difference of Barnosky and others (14,363 *E*/MS), and the blue diamond labeled '3' in Fig. 9B shows their extinction rate (28.7 *E*/MSY). Each is plotted versus the corresponding interval length of 500 years. The extinction difference and extinction rate of Barnosky and others both fall in the lower quartile of background differences and rates based on Cenozoic mammals, well below the median expectation for the time interval involved.

Finally, Loehle and Eschenbach (2012) calculated the rate of mammal species extinctions on islands. Rates of extinction on islands are generally acknowledged to be higher than rates in other settings:

$$\frac{58\ extinctions}{787\ total\ species}\cdot 10^6\ species \Big/ 500\ years = 147.4\ E \Big/ MSY \quad (6)$$

The blue diamond labeled '4' in Fig. 9A shows the extinction difference of Loehle and Eschenbach (73,698 *E*/MS), and the blue diamond labeled '4' in Fig. 9B shows their extinction rate (147.4 *E*/MSY). Each is plotted versus its corresponding interval length of 500 years. The extinction difference and extinction rate of Loehle and Eschenbach fall near the top of the lower quartile of background differences and rates based on Cenozoic mammals. When compared to expectation for the same scale of time, each is again well below the median background extinction rate for Cenozoic mammals. Comparing rates on the same scale of time, the island rates of Loehle and Eschenbach are substantially higher than those reported by Barnosky et al., (2011).

Fig. 9B shows modern extinction rates for mammals to be lower, not higher, than most background extinction rates when the latter are projected to the same scale of time. We study mammalian species and change in the modern world on a much shorter scale of time than is possible in the geological past. Extinction rates today could be higher than those in the geological past, but comparisons on the same scale of time do not support this idea. Foote (2000) developed a per-capita extinction-rate q based on boundary crossing that was said to be independent of interval length. However, testing on the PBDB ranges analyzed here shows q to have the inverse relationship to interval length shown in Fig. 9.

3. Discussion

The nine empirical studies analyzed here represent the range of relationships between intervals of time, differences, and rates of change (*I*, *D*, and *R*, respectively) that can be expected in geological settings. Two studies, one of creep on the San Andreas Fault and the other on anthropogenic carbon emissions, yield differences that are proportional to their associated time intervals, and yield rates that are consequently independent of their denominators. Two studies at the other extreme, one of radionuclide calibration of outcrop and basin erosion and the other of species extinctions, yield the opposite: differences that are largely independent of their time intervals, and rates that are consequently almost entirely dependent on their denominators. This contrast is expressed most clearly in the associated LDI and LRI temporal scaling slopes, which are high for directional processes with rates independent of their time scale, and low for stationary processes with rates dependent on their time scale.

4. Geological rates and the passage of time

What makes one process directional and another stationary? Why are temporal scaling slopes high in some studies and low in others? Table 2 summarizes the LDI and LRI slopes and intercepts for each of the nine studies reviewed here. Each study is interpreted in light of a model, directional, random, stationary, or intermediate, based on the associated LDI and LRI slopes. Table 2 also lists values for the range of LI values (minimum and maximum); for LI, LD, and LR spans; for LD and LR residuals; and for LI − LD and LImax − LD residual differences. All spans and differences are expressed in $\log_{10}$ or order-of-magnitude units. Three studies represent geological processes in historical times (fault creep, carbon emissions, and glacial advance), with longest intervals of $10^{1.65} = 45$ years, $10^{1.77} = 59$ years, and $10^{2.11} = 128$ years, respectively. The remaining studies are deeper in time, with longest intervals ranging from $10^{5.88} = 756$ thousand years (radionuclide calibration of outcrop and basin erosion) to $10^{9.00}$ = one billion years (sediment accumulation).

LDI and LRI slopes provide the same information about change because they are co-dependent. An LRI slope is always one unit more negative than the corresponding LDI slope. High LDI and LRI slopes, such as 0.978 and −0.022, respectively, in study 1 (fault creep), or 1.001 and 0.001 in study 2 (carbon emissions), are the marks of directional processes (as we saw from the time series in Figs. 1A and 2A). In contrast, LDI and LRI slopes are at or near 0.000 and −1.000, respectively, in study 7 (radionuclide calibration of outcrop and basin erosion) and study 9 (species extinction). LDI and LRI slopes at or near 0.000 and −1.000 are the marks of stationary processes. The outcrop and basin erosion process is stationary in the sense that there is little or no net change or difference in erosion amount as intervals lengthen in Fig. 7A. The extinction process is stationary in the sense that there is no net change of proportional extinction *E*/MS as intervals lengthen in Fig. 9A.

Five studies in Table 2 have a span of LI values greater than the corresponding span of LD values. These are studies 3 and 4 and studies 6 through 8. An LI span greater than an LD span means that the corresponding LI − LD difference is positive. Positive span differences shown in Fig. 10A range in value from 0.57 orders of magnitude in study 3 (glacial advance) to 4.64 orders of magnitude in study 8 (temperature change). Four studies have a span of LI values less than the span of LD values, which means that their span differences are negative. The four negative span differences in Fig. 10A range from −2.31 orders of magnitude in study 5 (tectonic uplift and exhumation) to −0.13 orders of magnitude in study 9 (species extinction). A linear model fit to all nine points in Fig. 10A has a slope of −0.099 (significantly different from a slope of zero) and an intercept of 0.53 on the LDI slope scale (−0.47 on the LRI slope scale). The coefficient of determination is $r^2 = 0.35$, which means that about 35% of the variation in LDI and LRI slopes can be attributed to the LI span − LD span difference.

A similar but narrower comparison can be made between the maximum LI value in a study and the corresponding span of LD or LR residuals (Table 2). Eight studies, 2 through 9, have LImax – LD residual differences that are positive. These are shown graphically in Fig. 10B, where the positive differences range from a low of 0.56 orders of magnitude in study 3 (glacial advance) to a high of 7.25 orders of magnitude in study 6 (river incision). One study, study 1 (fault creep), has an LImax – LD residual difference that is negative (−1.25). A linear fit to all nine points in Fig. 10B has a slope of −0.083 (significantly different from a slope of zero) and an intercept of 0.68 on the LDI slope scale (−0.32 on the LRI slope scale). The coefficient of determination is $r^2 = 0.42$, which means that about 42% of the variation in LDI and LRI slopes can be attributed to the LImax – LD residual span difference.

Fig. 10A shows that LDI and LRI slopes are higher when the LI span − LD span is negative (LI span < LD span; Fig. 10A). This is also true when

Table 2
Comparison across studies of log_{10} difference versus interval (LDI) slopes, log_{10} rate versus interval (LRI) slopes, model process interpretations based on the slopes, and corresponding intercepts. Also included are ranges or spans of log_{10} intervals, differences, and rates (LI, LD, and LR), and of LD and LR residuals. Differences are included for the LI span − LD span difference and for the LImax – LD residual span difference (see Fig. 10). Entries in columns with asterisks are in orders of magnitude.

Study	LDI slope	LRI slope	Model process interpretation	LDI and LRI intercept < yr>	LImin*	LImax*	LI span*	LD span*	LR span*	LD and LR resid.*	LI − LD*	LImax − LD resid.*
1. Fault creep (mm)	0.978	−0.022	Directional	1.269	−1.86	1.65	3.51	4.41	2.91	2.90	−0.90	−1.25
2. Carbon emissions (PgC)	1.001	0.001	Directional	0.768	0.00	1.77	1.77	2.18	0.62	0.62	−0.40	1.16
3. Glacial advance and retreat (m)	0.173	−0.827	Stationary	2.169	0.00	2.11	2.11	1.54	2.38	1.55	0.57	0.56
4. Sediment accumulation (mm)	0.392	−0.608	Random	1.934	−5.80	9.00	14.80	11.00	11.60	7.60	3.80	1.40
5. Uplift and exhumation (mm)	0.722	−0.278	Direct.-Rand.	1.031	−0.70	8.50	9.20	11.51	8.22	7.47	−2.31	1.03
6. River incision (mm)	0.449	−0.551	Random	2.796	6.00	7.48	1.48	0.73	0.89	0.23	0.75	7.25
7. Outcrop and basin erosion (cm)	0.020	−0.980	Stationary	1.709	2.64	5.88	3.24	0.18	3.10	0.15	3.06	5.73
8. Temperature change (°C)	0.120	−0.880	Stationary	−0.058	1.18	7.70	6.52	1.88	5.10	1.31	4.64	6.39
9. Species extinction (E/MS)	0.000	−1.000	Stationary	5.620	5.06	7.78	2.72	2.85	4.91	2.85	−0.13	4.93

*Intervals, spans, residuals, and span differences are expressed as orders of magnitude.

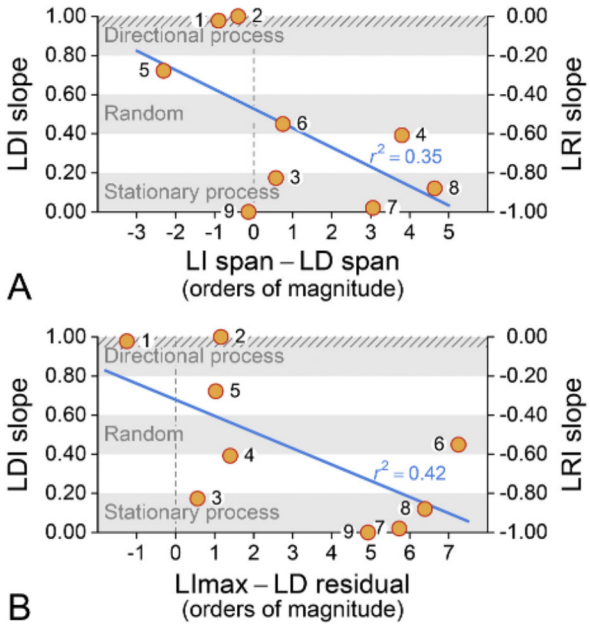

Fig. 10. LDI and LRI slopes for the nine case studies analyzed here, shown in relation to the ranges or spans of observation on the LDI and LRI plots of Figs. 1 through 9. (A) LDI and LRI slopes in relation to the difference between the spans of LI and LD. (B) LDI and LRI slopes in relation to the difference between the maximum value of LI and the span of LD residuals. Directional processes with high LDI and LRI slopes have change and the acquisition of difference balanced by the passage of time. Random and stationary processes with medium and low LDI and LRI slopes have more constrained change and acquisition of difference and do not keep pace with the passage of time. Directional processes with LDI slopes greater than 0.95 and LRI slopes greater than −0.05 (hatched) have rates that are largely independent of their denominators. Non-directional processes with lower temporal scaling slopes have rates that are dependent on their denominators and can only be compared on a common scale of time. Blue lines are fit to the nine points in each panel: $r^2 = 0.35$ and Pr (slope = 0) is 0.048 (one-tailed test) in panel A; $r^2 = 0.42$ and Pr (slope = 0) is 0.030 (one-tailed test) in panel B. (For interpretation of the references to colour in this figure legend, the reader is referred to the web version of this article.)

the LImax − LD residual span is negative (LImax < LD residual span; Fig. 10B). Conversely, LDI and LRI slopes are lower when the LI span exceeds the LD span, and when LImax values exceed LD residual spans. Many of the geological changes that we quantify as differences and rates are more constrained than the passage of time. The distance a fault can creep or a glacier can advance is relatively limited on the surface of the earth. Similarly, the supply of sediment and the space to accumulate it, the elevations associated with tectonic uplift and exhumation, and the depth of river incision are all constrained by the relatively limited flexure and relief of the earth's surface. Radionuclide calibrations of erosion differences are more or less constant over the range of their associated intervals. Temperatures change through a relatively narrow range of values. Finally, empirically, extinctions are a highly variable proportion of a biota, but the LD and LD residual spans range through less than three orders of magnitude of a much longer history. When intervals of time exceed the change that is possible for a difference of interest, then time soon dominates a quotient of the two.

Directional change indicates a balance between the acquisition of difference and the passage of time. One increases as a more or less constant proportion of the other. The result, when graphed on logarithmic axes, is an LDI plot with a slope close to 1.000. A rate is difference divided by time (or, when logged, LD – LI), which, for directional change, yields an LRI plot with a slope close to 0.000. When the acquisition of difference is constrained by limits, so the cumulative difference lags time as a proportion, then the change becomes random or even stationary and the resulting LDI and LRI slopes are correspondingly less positive. This can happen when a process oscillates between extremes, as the time series for the Ghulkin Glacier does in Fig. 3A. It can also happen on a finer scale when, for example, short-term dynamics of episodic deposition and reworking explain the longer-term temporal scaling of sediment accumulation (Fig. 4; Sadler, 1981).

5. Comparison of rates on a common time scale

How can rates calculated on different scales of time be compared? Rates in each of the studies reviewed here are not wrong as they were calculated, but many of the rates are incomplete and mean little as stand-alone rates separated from their denominators. The model for rate calculation is implicitly a directional time series like the examples of fault creep in Fig. 1 and anthropogenic carbon emissions in Fig. 2. When a time series is directional, then differences increase in proportion to time and rates appropriately remove this effect. However, time series in geological settings are not always directional, and the independence of rates from their denominators must be investigated and documented in each case. LDI and LRI temporal scaling provides an efficient test of independence and a reliable indicator of dependence.

Every rate has a denominator, the time scale of its calculation. Woerd et al. (2006) calculated an average creep or slip rate for the San Andreas

Fault of 15.9 mm per year on a time scale of 35,500 years. The rate 15.9 mm / yr does not stand alone but has an associated time scale of 35,500 years. Adding the index in chevrons, the rate can be written as 15.9 mm / yr <35,500 yr>. The Revenaugh and Reasoner (1997) San Andreas creep rate, written similarly, is 13.6 mm / yr < 23.1 my>. Each is calculated on a different scale of time, and we can only justify comparison when we know that creep on the San Andreas Fault is directional and consistent with both longer-term rates. Indexing a rate by its time scale — following a rate by its denominator, in chevrons to set it apart — is a reminder that any comparison of rates must be limited to those calculated on the same time scale, or limited, when temporal scaling is adequately known, to rates projected to the same time scale.

One common and misleading approach to comparison of rates is illustrated in Fig. 9 for extinction. It involves three steps. First, pooling samples representing short-term rates such as the points labeled 2, 3, and 4 enclosed in the blue rectangle in Fig. 9B (where mean LR = 1.72). Second, pooling a corresponding range of long-term rates such as the background rates from the fossil record enclosed in the red rectangle in Fig. 9B (where mean LR = −1.43). And, finally, comparing the two sets of rates directly, without considering differences in the underlying scales of time involved. Direct comparison as stand-alone rates suggests that 400–500 year historical extinction rates are 1.72 − −1.43 = 3.15 orders of magnitude higher than background extinction rates in the fossil record. Reasoning this way, many studies have found historical rates of extinction to be orders of magnitude higher than background rates (Pimm et al., 2006; Regan et al., 2001; Barnosky et al., 2011; Loehle and Eschenbach, 2012; Rounsevell et al., 2020). These studies ignore differences in the scales of time associated with each calculated rate. They assume, implicitly (and erroneously), that calculating rates somehow corrects for differing denominators and permits comparison on different scales of time.

Fig. 9 shows too how temporal scaling can be used to project differences and rates to the same time scale for comparison. Projection of long-term extinction LD values in relation to LI (solid blue median and dashed blue quartile lines in Fig. 9A) indicates that extinction differences on historical scales of time (diamonds in the blue rectangle in Fig. 9A) are generally similar to background extinction differences on geological scales of time (red rectangle in Fig. 9A). Similarly, projection of extinction LR values in relation to LI (solid blue median and dashed blue quartile lines in Fig. 9B) indicates that we should expect background extinction rates to be much higher on the 400–500 year time scale of historical extinctions than they are on the million- to multimillion-year time scales of their original calculation. The mean LR = 1.72 for 400–500 year historical extinctions (blue rectangle in Fig. 9B) is well within the range projected by temporal scaling of background extinctions (red rectangle in Fig. 9B). The historical extinctions are more than an order of magnitude lower, not higher, than the median LR of 2.97 for a 450-year interval predicted from temporal scaling of background rates.

6. Conclusion

The Kukal (1990) book-length review on *The Rate of Geological Processes* hinted that our understanding of geological rates changed in the 1980s, with Reineck (1960) and Sadler (1981) as catalysts. However, now forty years later, the idea that geological rates are dependent on their denominators is still not as widely appreciated and embraced as it should be. The inverse scaling of rates and intervals that Sadler documented (Fig. 4B) is sometimes called a "measurement-interval bias" (Gardner et al., 1987), a "Sadler effect" (Romans, 2007), or a "time-scale bias" (Ganti et al., 2016). 'Bias' and 'effect' are ambiguous and often belittling — as they seem to be here. What is important is that all but the most directional processes yield rates dependent on their denominators. This is a common problem in geology where geophysical, geochemical, sedimentological, environmental, and biological changes or differences of interest are often constrained to a relatively narrow range of possibilities compared to the very long intervals of time available in earth history. Observed changes or differences are sometimes simply overwhelmed by the passage of time. Temporal scaling is necessary to determine when this is important. If rates cannot be shown to be independent of their denominators, then any comparison of rates must be restricted to, or projected to, a common scale of time.

Declaration of Competing Interest

None.

Acknowledgments

I thank Tobias Bolch for providing the measurements plotted in Fig. 3A, Peter Sadler for information on the rates in Fig. 4B, Thomas Gardner for responding to a request for data, and Bruce Wilkinson for numbers analyzed in Fig. 5. John Alroy compiled the species ranges analyzed by Foote and Raup, and many of the species ranges in the Paleobiology Database analyzed here. Cenozoic mammal ranges were downloaded from the Paleobiology Database on June 19, 2020. Finally, I thank Stuart Pimm for a helpful discussion of extinction rates, and Shanan Peters, Peter Sadler, and Bruce Wilkinson for thoughtful reviews that improved the manuscript substantially.

References

Aadland, T., Sadler, P.M., Helland-Hansen, W., 2018. Geometric interpretation of time-scale dependent sedimentation rates. Sediment. Geol. 371, 32–40.
Barnosky, A.D., Matzke, N., Tomiya, S., Wogan, G.O.U., Swartz, B., Quental, T.B., Marshall, C., McGuire, J.L., Lindsey, E.L., Maguire, K.C., Mersey, B., Ferrer, E.A., 2011. Has the Earth's sixth mass extinction already arrived? Nature 471, 51–57.
Bolch, T., Kulkarni, A., Kääb, A., Huggel, C., Paul, F., Cogley, J.G., Frey, H., Kargel, J.S., Fujita, K., Scheel, M., Bajracharya, S., Stoffel, M., 2012. The state and fate of Himalayan glaciers. Science 336, 310–314.
Dickens, G.R., O'Neil, J.R., Rea, D.K., Owen, R.M., 1995. Dissociation of oceanic methane hydrate as a cause of the carbon isotope excursion at the end of the Paleocene. Paleoceanography 10, 965–971.
Dunai, T.J., 2010. Cosmogenic Nuclides: Principles, Concepts and Applications in the Earth Surface Sciences. Cambridge University Press, Cambridge, 187 pp.
Finnegan, N.J., Schumer, R., Finnegan, S., 2014. A signature of transience in bedrock river incision rates over timescales of 10^4–10^7 years. Nature 505 (7483), 391–394.
Foote, M., 2000. Origination and extinction components of taxonomic diversity: general problems. Paleobiology 26 (S4), 74–102.
Foote, M., Raup, D.M., 1996. Fossil preservation and the stratigraphic ranges of taxa. Paleobiology 22, 121–140.
Friedlingstein, P., Jones, M.W., O'Sullivan, M., Andrew, R.M., Hauck, J., Peters, G.P., Peters, W., Pongratz, J., Sitch, S., Le Quéré, C., Bakker, D.C.E., Canadell, J.G., Ciais, P., Jackson, R.B., Anthoni, P., Barbero, L., Bastos, A., Bastrikov, V., Becker, M., Bopp, L., Buitenhuis, E., Chandra, N., Chevallier, F., Chini, L.P., Currie, K.I., Feely, R. A., Gehlen, M., Gilfillan, D., Gkritzalis, T., Goll, D.S., Gruber, N., Gutekunst, S., Harris, I., Haverd, V., Houghton, R.A., Hurtt, G., Ilyina, T., Jain, A.K., Joetzjer, E., Kaplan, J.O., Kato, E., Klein Goldewijk, K., Korsbakken, J.I., Landschützer, P., Lauvset, S.K., Lefèvre, N., Lenton, A., Lienert, S., Lombardozzi, D., Marland, G., McGuire, P.C., Melton, J.R., Metzl, N., Munro, D.R., Nabel, J.E.M.S., Nakaoka, S.I., Neill, C., Omar, A.M., Ono, T., Peregon, A., Pierrot, D., Poulter, B., Rehder, G., Resplandy, L., Robertson, E., Rödenbeck, C., Séférian, R., Schwinger, J., Smith, N., Tans, P.P., Tian, H., Tilbrook, B., Tubiello, F.N., van der Werf, G.R., Wiltshire, A.J., Zaehle, S., 2019. Global carbon budget 2019. Earth System Science Data 11 (4), 1783–1838.
Gani, N., Gani, M.R., Abdelsalam, M., 2007. Blue Nile incision on the Ethiopian Plateau: Pulsed plateau growth, Pliocene uplift, and hominin evolution. GSA Today 17 (9), 4–11.
Ganti, V., von Hagke, C., Scherler, D., Lamb, M.P., Fischer, W.W., Avouac, J.-P., 2016. Time scale bias in erosion rates of glaciated landscapes. Sci. Adv. 2 (10), e1600204.
Gardner, T.W., Jorgensen, D.W., Shuman, C., Lemieux, C.R., 1987. Geomorphic and tectonic process rates: effects of measured time interval. Geology 15 (3), 259–261.
Gingerich, P.D., 1983. Rates of evolution: effects of time and temporal scaling. Science 222 (4620), 159 161.
Gingerich, P.D., 1993. Quantification and comparison of evolutionary rates. Am. J. Sci. 293 (A), 453–478.
Gingerich, P.D., 2009. Rates of evolution. Annu. Rev. Ecol. Evol. Syst. 40, 657–675.
Gingerich, P.D., 2019a. Rates of Evolution: A Quantitative Synthesis. Cambridge University Press, Cambridge, 381 pp.
Gingerich, P.D., 2019b. Temporal scaling of carbon emission and accumulation rates: modern anthropogenic emissions compared to estimates of PETM-onset accumulation. Paleoceanogr. Paleoclimatol. 34 (3), 329–335.
Hewitt, K., 2011. Glacier change, concentration, and elevation effects in the Karakoram Himalaya, upper Indus Basin. Mt. Res. Dev. 31 (3), 188 200 (13).

Jerolmack, D.J., Sadler, P., 2007. Transience and persistence in the depositional record of continental margins. J. Geophys. Res. Earth Surf. 112, F03S13.
Kemp, D.B., Eichenseer, K., Kiessling, W., 2015. Maximum rates of climate change are systematically underestimated in the geological record. Nat. Commun. 6 (8890), 1–6.
Kukal, Z., 1990. The rate of geological processes. Earth Sci. Rev. 28 (1 3), 1 284.
Lal, D., 1991. Cosmic ray labeling of erosion surfaces: in situ nuclide production rates and erosion models. Earth Planet. Sci. Lett. 104 (2), 424–439.
Loehle, C., Eschenbach, W., 2012. Historical bird and terrestrial mammal extinction rates and causes. Divers. Distrib. 18 (1), 84–91.
Partin, C.A., Sadler, P.M., 2016. Slow net sediment accumulation sets snowball Earth apart from all younger glacial episodes. Geology 44 (12), 1019–1022.
Pimm, S., Raven, P., Peterson, A., Şekercioğlu, Ç.H., Ehrlich, P.R., 2006. Human impacts on the rates of recent, present, and future bird extinctions. Proceed. Nat. Acad. Sci. USA 103 (29), 10941–10946.
Portenga, E.W., Bierman, P.R., 2011. Understanding Earth's eroding surface with ^{10}Be. GSA Today 21 (8), 4–10.
Regan, H.M., Lupia, R., Drinnan, A.N., Burgman, M.A., 2001. The currency and tempo of extinction. Am. Nat. 157 (1), 1–10.
Reineck, H.-E., 1960. Über Zeitlücken in Rezenten Flachsee-Sedimenten [on time gaps in recent shallow-sea sediments]. Geol. Rundsch. 49 (1), 149 161.
Revenaugh, J., Reasoner, C., 1997. Cumulative offset of the San Andreas fault in Central California: a seismic approach. Geology 25 (2), 123–126.
Romans, B., 2007. Sediment accumulation rates and bias: the Sadler effect. Wired.com Science 2007, 1–5.
Rounsevell, M.D.A., Harfoot, M., Harrison, P.A., Newbold, T., Gregory, R.D., Mace, G.M., 2020. A biodiversity target based on species extinctions. Science 368 (6496), 1193–1195.
Sadler, P.M., 1981. Sediment accumulation rates and the completeness of stratigraphic sections. J. Geol. 89 (5), 569–584.
Sadler, P.M., Jerolmack, D.J., 2015. Scaling laws for aggradation, denudation and progradation rates: the case for time-scale invariance at sediment sources and sinks. Geol. Soc. Lond., Spec. Publ. 404 (1), 69–88.
Schlager, W., Marsal, D., Geest, P.A.G.V.D., Sprenger, A., 1998. Sedimentation rates, observation span, and the problem of spurious correlation. Math. Geol. 30 (5), 547 556.
Schulz, S.S., 1989. Catalog of creepmeter measurements in California from 1966 through 1988. In: U. S. Geological Survey Open-File Report, 89-650, pp. 1–193.
Sheets, H.D., Mitchell, C.E., 2001. Uncorrelated change produces the apparent dependence of evolutionary rate on interval. Paleobiology 27, 429–445.
Sieh, K.E., Jahns, R.H., 1984. Holocene activity of the San Andreas fault at Wallace Creek, California. Geol. Soc. Am. Bull. 95 (8), 883–896.
Wilkinson, B.H., McElroy, B.J., Kesler, S.E., Peters, S.E., Rothman, E.D., 2009. Global geologic maps are tectonic speedometers — rates of rock cycling from area-age frequencies. Geol. Soc. Am. Bull. 121 (5–6), 760–779.
Woerd, J.V.D., Klinger, Y., Sieh, K., Tapponnier, P., Ryerson, F.J., Mériaux, A.-S., 2006. Long-term slip rate of the southern San Andreas Fault from 10Be-26Al surface exposure dating of an offset alluvial fan. J. Geophys. Res. Solid Earth 111 (B4).
Zachos, J.C., Pagani, M., Sloan, L.C., Thomas, E., Billups, K., 2001. Trends, rhythms, and aberrations in global climate 65 Ma to present. Science 292 (5517), 686–693.